UC Irvine
UC Irvine Electronic Theses and Dissertations

Title
Face processing evokes high frequency activity (80-500 Hz) in localized regions of the brain

Permalink
https://escholarship.org/uc/item/6b70871m

Author
Caliboso, Walter

Publication Date
2015

Peer reviewed|Thesis/dissertation

eScholarship.org Powered by the California Digital Library
University of California

UNIVERSITY OF CALIFORNIA,
IRVINE

Face processing evokes physiological high frequency activity (80-500 Hz) in localized regions of the brain

THESIS

submitted in partial satisfaction of the requirements
for the degree of

MASTER OF SCIENCE

in Biomedical Engineering

by

Walter Caliboso

Thesis Committee:
Assistant Professor Beth Lopour, Chair
Associate Professor Jack Lin
Professor Ramesh Srinivasan

2015

© 2015 Walter Caliboso

TABLE OF CONTENTS

LIST OF FIGURES

LIST OF TABLES

ACKNOWLEDGMENTS

Without the help of numerous individuals, this thesis and research would not be possible. First, I would like to express the deepest appreciation to my committee chair, Dr. Beth Lopour. Her encouragement, guidance, and persistent help were instrumental in its completion. Furthermore, I would like to thank my committee members, Dr. Jack Lin and Dr. Ramesh Srinivasan, for their encouragement and useful feedback.

I would also like to thank my fellow graduate students Vaibhav Bajaj and Krit Charupanit for the stimulating discussions and help with data analysis and programming. Also, special thanks to Dr. Jeffrey Riley and Jie Zheng for helping with electrode localization and data collection.

Finally, I want to express my deepest gratitude to my family for their unconditional love and support.

ABSTRACT OF THE THESIS

Face processing evokes physiological high frequency activity (80-500 Hz) in localized regions of the brain

By

Walter Caliboso

Master of Science in Biomedical Engineering

University of California, Irvine, 2015

Assistant Professor Beth Lopour, Chair

Here we investigate high frequency activity (HFA) evoked during face perception in humans. The purpose of this research are: (1) to develop and validate an automatic HFA detector, (2) to determine whether HFA is increased during face processing, and (3) to compare the characteristics of HFAs between baseline and activation conditions.

Twelve subjects undergoing clinical evaluation for epilepsy surgery passively viewed a paradigm to activate face-sensitive regions in the brain. The paradigm consisted of alternating 24-second blocks of baseline (landscapes) and activation (faces) video clips for a total of 16 blocks. Target locations for the implanted electrodes were determined solely for the purpose of seizure localization. A total of 465 bipolar signals were analyzed after excluding electrodes within the seizure onset zone and anatomical defects and those having excessive noise. We compared the rate of HFAs during viewing of landscapes versus faces. In 14 sites across four subjects, we found a significant increase in HFA rates during face viewing. Some sites corresponded to regions previously associated with face processing while additional sites were located in frontal regions. These findings may provide important information about the activity of brain regions during face processing that cannot be inferred from phase-locked ERPs.

1 Introduction

1.1 Face Perception

Face processing is a highly developed skill in humans. Functional imaging work has characterized the neural basis of face perception and identified brain regions that preferentially respond to faces and contribute to human's face processing proficiencies (Collins and Olson, 2014). Among these regions, a hierarchical organization branching from core regions to an extended system for visual analysis of faces has been proposed (Haxby et al., 2000). The core system -- the inferior occipital gyri, the lateral fusiform gyrus, and the superior temporal sulcus – appears to be involved in the early perception of facial features, changeable aspects of faces, and perception of unique identity, whereas the extended system consisting of the amygdala and insula are tuned to emotional aspects of facial expression (Figure 1) (Haxby et al., 2000; Weiner and Grill-Spector, 2015).

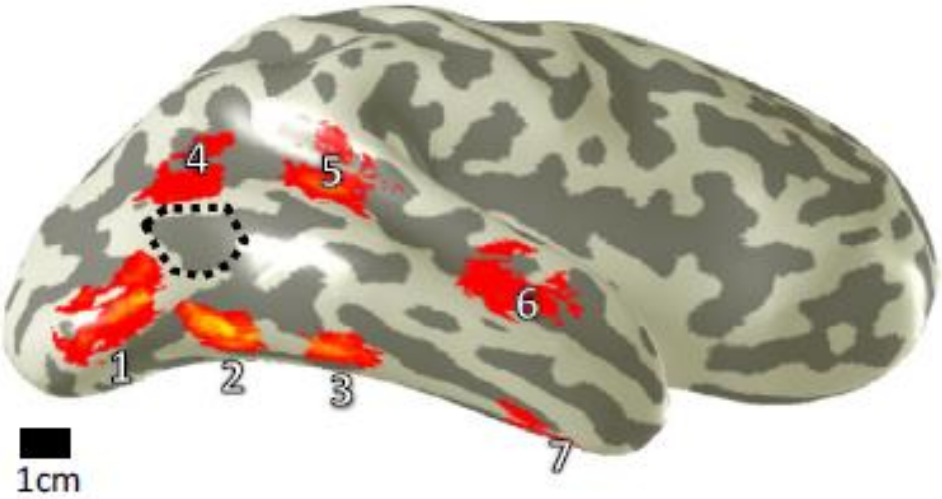

Figure 1. Cortical surface of a human brain (Wiener and Grill-Spector, 2015). Warm colors indicate face-selective regions (Weiner and Grill-Spector, 2015).1 – Inferior Occipital Gyrus or Occipital Face Area; 2 – Posterior Fusiform Face Area; 3 – Mid-

Fusiform Face Area; 4 – Posterior Superior Temporal Sulcus; 5 – Mid-Superior Temporal Sulcus; 6 – Anterior Superior Temporal Sulcus; 7 – Anterior Temporal Face Area. Dotted black line – human motion-selective complex.

With functional imaging studies, the brain regions that participate in face perception could be studied non-invasively in the normal human brain with excellent anatomical precision. In these regions, the activity in response to faces is greater than that evoked by the perception of control stimuli or by non-face objects (Haxby et al., 2000). However, imaging studies such as functional Magnetic Resonance Imaging (fMRI) and Positron Emission Tomography (PET) have poor temporal resolution and is thus unable to accurately capture the finer time-dependent aspects of visual processing (Engel and McCarthy, 2011). In contrast, electrophysiological recordings can provide excellent temporal resolution but are invasive and have limited spatial coverage (Cohen, 2014). These recordings provide a unique opportunity to investigate the neural correlates of normal cognitive functions such as face processing (Kucewicz et al., 2014).

1.2 Intracranial EEG and High Frequency Activity

Electrophysiological recordings have been traditionally characterized by their dominant frequency bands. In general, these bands are designated as delta (2-4 Hz), theta (4-8 Hz), alpha (8-12 Hz), beta (12-30), and gamma (> 30 Hz) (Cohen, 2014). However, technological advances have allowed researchers to record data at a higher rate, leading to the discovery of transient oscillations with frequencies beyond the gamma band. Although no standard definitions of high frequency oscillations (HFOs) exist, these oscillations have been labeled by many as ripple (80 - 250 Hz), fast ripple (250-500 Hz), and sigma (>600 Hz) (Staba et al., 2014). This study determines whether

transient ripple and fast ripple activity are induced during cognitive processing, specifically face perception.

High frequency activity (HFA) have been established as an index of cortical processing not only in sensory and motor cortices, but also in any cortical region that is involved by a task (Lachaux et al., 2012). These transient events have been linked to cognitive processes such as memory, language production and perception, and face perception. High frequency oscillations are subsets of HFAs and have been the focus of recent studies due to their association with normal and diseased brain functions (Matsumoto et al., 2013). Initial observations have linked gamma oscillations to coordination of cortical processing during vision, language and motor functions, and ripple oscillations to memory functions (Gray and Singer 1989; Crone et al. 2011; Buzsaki et al., 1992). Meanwhile, fast ripples were thought to be a specific biomarker for epilepsy (Bragin et al., 1999b). However, other studies have also found increased rates of gamma and ripple oscillations in human epileptogenic hippocampus (Crepon et al., 2010), while fast ripples were also linked to physiological somatosensory evoked HFAs (Baker et al., 2003). Therefore, the frequency of HFOs does not seem to distinguish whether it is pathological or physiological, and distinguishing between pathological HFOs and HFOs associated with normal cognitive function remains a challenge (Matsumoto et al., 2013a).

Lachaux and colleagues propose referring to high frequency activity as “neural oscillations” only when there is evidence that the activity is rhythmic, or a collection of several rhythmic processes (2012). This study used a detector to identify transient high

frequency activity in the ripple and fast ripple band, regardless of whether they were HFOs or not.

Several studies have used intracranial electroencephalogram (EEG) recordings to provide a spatially and temporally resolved investigation of the face perception system (Allison et al., 1994; Puce et al., 1999). For example, recordings in humans from subdural electrodes placed on the fusiform gyrus and nearby locations within the ventral occipitotemporal cortex (VOTC) have revealed a face-specific event-related potential (ERP) that appears as a cortical surface-negative potential that peaks at ~200 ms (face-N200) after the onset of face stimulus (Allison et al., 1994). However, the scope of these studies was limited to the electrical potentials phase-locked to visual stimuli or to a limited view of the EEG spectrum (Klopp et al., 1999). Lachaux and colleagues expanded the face processing EEG spectrum to the gamma band, where they found oscillations (>30 Hz) induced during face perception and recorded from electrodes along the VOTC (Lachaux et al., 2005). While these studies have provided information about localized information processing in the brain, this signal-averaging approach may discard oscillatory potentials that are not phase-locked across trials (Engel and McCarthy, 2011).

1.3 Aims

Here we investigate induced high frequency activity during face perception. This investigation aims to identify the face processing regions based on the rate of transient high frequency events using techniques generally implemented in epilepsy research. The findings may provide important information about the activity of brain regions during

face processing that cannot be inferred from phase-locked ERPs. Specifically, the aims of this research are:

1. Develop, validate, and optimize an automatic detector that can identify high frequency activity,
2. Test the hypothesis that there is an increased rate of high frequency activity in brain regions involved during face processing,
3. Test whether characteristics of HFAs such as amplitude, peak frequency, and duration differ when they occur during activation or baseline conditions.

2 Method

2.1 Subjects

This study included twelve subjects with pharmacoresistant epilepsy (mean age ± standard deviation: 32.4 ± 9.2, female: 5, Temporal Lobe Epilepsy (TLE): 8) admitted for intracranial EEG monitoring as part of surgical treatment. All subjects were informed about the study goals by the experimenter and provided with a written consent form. Target locations for the implanted electrodes were determined solely by the clinical requirements, with unequal distribution of implanted electrodes in the cortical and subcortical structures. Subject demographics, epilepsy type, and electrode target locations are shown in Table 1. This study was reviewed and approved by the Institutional Review Board of the University of California Irvine.

Table 1. Patient and electrode information. TLE: Temporal Lobe Epilepsy; FLE: Frontal Lobe Epilepsy.

Patient	Gender / Age	Epilepsy	Target Location	Electrode Type
1	F / 30	TLE	Frontal	1 x 6 Strip 8 x 8 Grid
			Orbitofrontal	1 x 6 Strip
			Occipital	1 x 6 strip
			Parietal	8 x 8 Grid
			Temporal	1 x 4 Strip (3)
2	M / 48	FLE	Frontal	1 x 6 Strip
			Orbitofrontal	1 x 6 Strip
			Temporal	1 x 8 Strip (2)
			Frontal / Parietal	8 x 8 Grid
			Interhemispheric	4 x 6 Grid
3	F / 22	TLE	Frontal	1 x 6 Strip (3)
			Temporal	1 x 6 Strip 1 x 4 Strip
			Amygdala	1 x 6 Depth
			Hippocampus	1 x 6 Depth
4	M / 24	TLE	Frontal	8 x 8 Grid 1 x 8 Depth 1 x 6 Depth
			Orbitofrontal	1 x 6 Strip

			Temporal	1 x 6 Strip (3)
			Amygdala	1 x 6 Depth
			Hippocampus	1 x 6 Depth
5	M / 38	TLE	Frontal	6 x 2 Grid 1 x 6 Strip (2)
			Temporal	4 x 8 Grid 1 x 4 Strip
			Amygdala	1 x 8 Depth
6	F / 35	FLE	Frontal	3 x 8 Grid 1 x 4 Strip
			Orbitofrontal	1 x 4 Strip
			Parietal / Frontal	8 x 8 Grid
			Temporal	1 x 4 Strip (2)
7	M / 23	TLE, Hippocampal onset	Temporal	4 x 8 Grid 1 x 4 Strip (2)
			Frontal	1 x 6 Strip
			Parietal	1 x 6 Strip
			Hippocampus	1 x 8 Depth
			Amygdala	1 x 8 Depth
8	M / 50	TLE	Temporal	8 x 8 Grid 1 x 6 Strip (2)
			Frontal	1 x 6 Strip
			Orbitofrontal	1 x 4 Strip
			Parietal	1 x 8 Strip
			Amygdala	1 x 8 Depth (2)
			Hippocampus	1 x 8 Depth (2)
9	F / 33	TLE	Hippocampus Head	1 x 10 Depth (2)
			Hippocampus Tail	1 x 10 Depth (2)
			Amygdala	1 x 10 Depth (2)
			Orbitofrontal	1 x 10 Depth (2)
			Anterior Cingulate	1 x 12 Depth
10	F / 32	TLE	Orbitofrontal	1 x 8 Depth 1 x 12 Depth
			Cingulate	1 x 12 Depth (4)
			Cuneus	1 x 12 Depth
			Amygdala	1 x 8 Depth
			Hippocampus	1 x 8 Depth
11	M / 28	TLE	Cingulate	1 x 12 Depth (4)
			Hippocampus	1 x 10 Depth (2) 1 x 12 Depth
			Amygdala	1 x 10 Depth 1 x 12 Depth
			Orbitofrontal	1 x 12 Depth
12	M / 26	TLE	Temporal	4 x 8 Grid (2) 1 x 6 Strip

			Frontal	1 x 6 Strip
			Amygdala	1 x 10 Depth
			Hippocampus	1 x 10 Strip (2)
			Orbitofrontal	4 x 5 Grid

2.2 Stimuli

This study used a face paradigm developed to activate face-sensitive regions in each subject (Schacher et al., 2006). Subjects sat upright in a hospital bed and viewed a video on a laptop computer. The video consisted of alternating 24 second blocks of baseline and activation for a total of 16 blocks (Figure 2). Baseline blocks consisted of 7-12 clips of 1-6 seconds each of dull domestic landscapes. These episodes were chosen for their lack of emotional content. On the other hand, activation blocks consisted of 7-12 clips of 1-6 seconds each from thriller and horror films. All episodes showed the faces of actors expressing fear with high intensity. Subjects were instructed to focus on the actor's eyes during the activation blocks. The intracranial EEG data from all available channels for each subject was recorded while the subject was passively viewing the face paradigm.

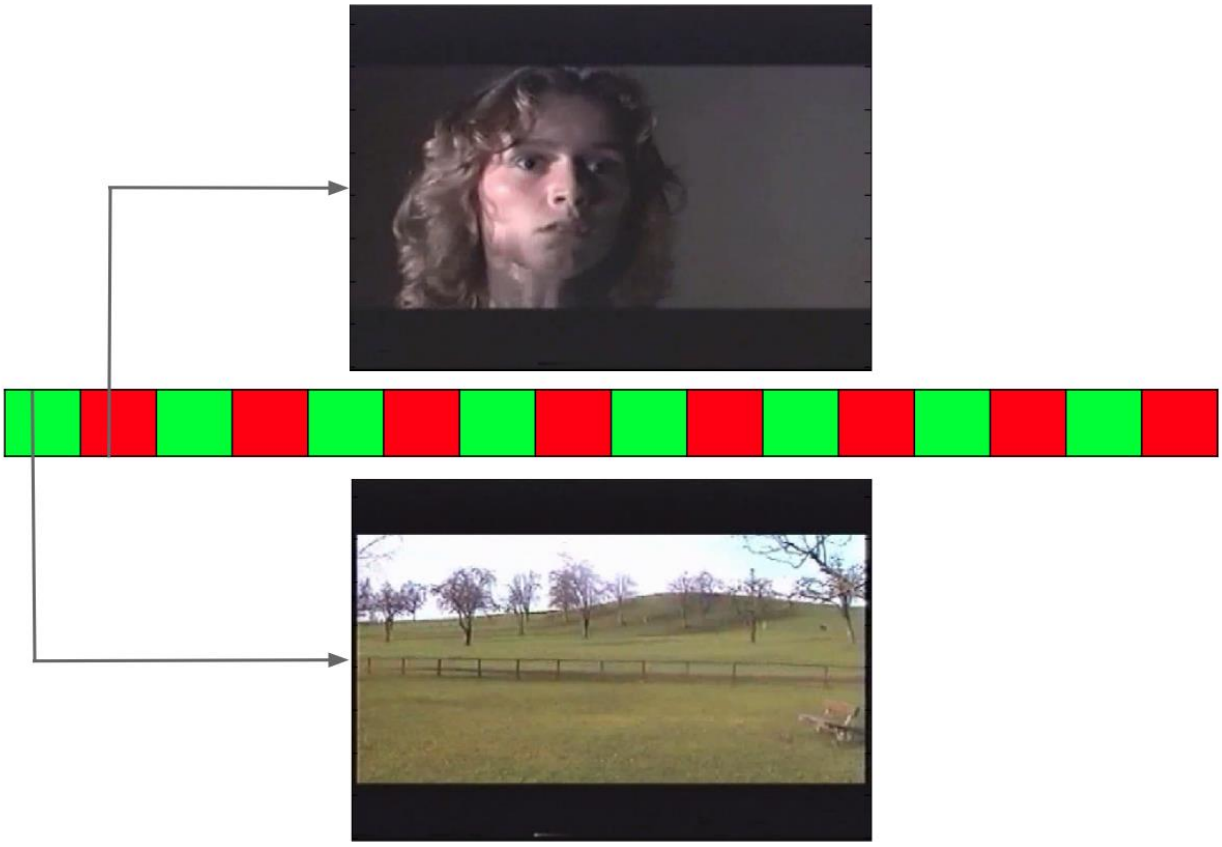

Figure 2. Examples of landscape and fearful face. Green: baseline blocks - landscape. Red: activation blocks - fearful faces. Each block is 24 seconds long and consists of 7-12 clips of either landscape or fearful faces.

2.3 Intracranial EEG Recording

Intracranial EEG were recorded with the standard strip, grid, or depth clinical electrodes and sampled at 5000 Hz (Nihon Kohden EEG-1200). Each subject's preimplantation MRI images and post implantation CT scan were co-registered to confirm the electrode locations.

2.4 Data Preparation

All analyses were performed in Matlab using custom-made code (Mathworks Inc.). Signals were re-referenced to a bipolar montage prior to any analysis. In this referencing method, one bipolar channel of data was created from every pair of adjacent electrodes. (Figure 3).

Electrodes that were part of the seizure-onset-zone (SOZ) and that had excessive noise were excluded from analysis. Epochs containing epileptiform spikes and sharp transients were visually identified and HFAs detected within these epochs were rejected.

This study analyzed 628 bipolar signals across twelve patients. Out of the 628, 163 signals were excluded due to the electrode's proximity to the seizure-onset-zone (129), anatomical defects (10), and having excessive noise (24). The remaining signals were taken from electrodes located in the frontal (179), temporal (110), orbitofrontal (47), cingulate (41), hippocampus (38), amygdala (22), parietal (13), cuneus (12), and occipital (3) regions.

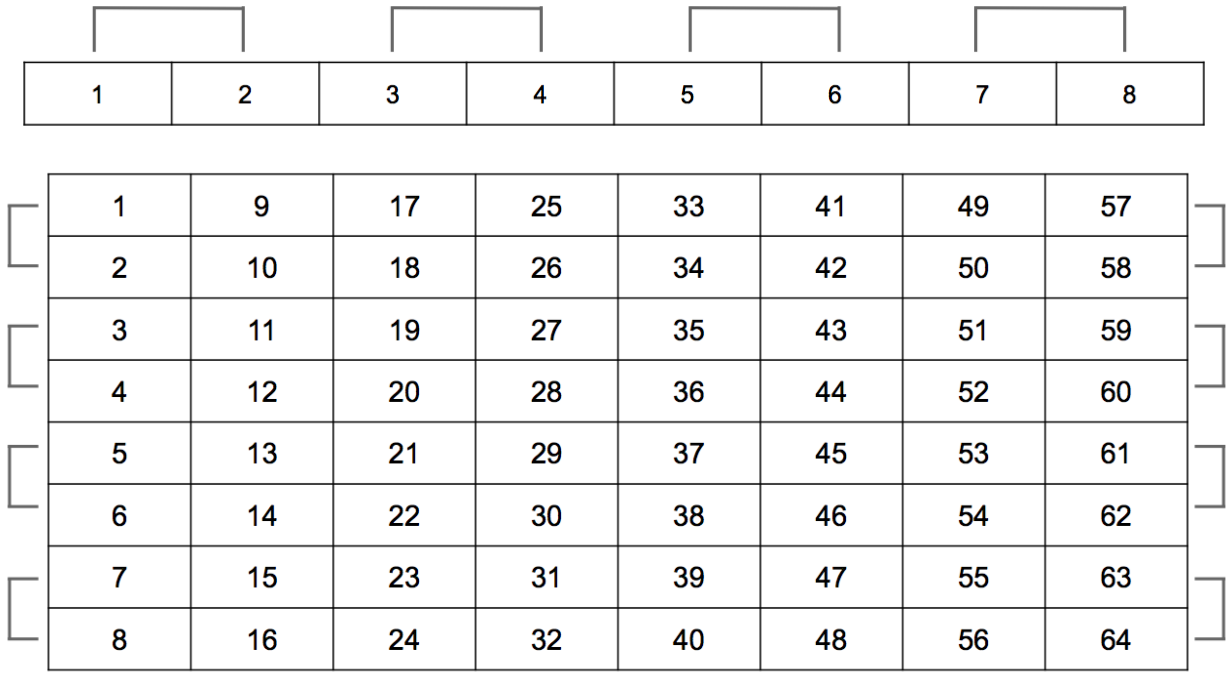

Figure 3. Bipolar referencing of broadband signals. Each numbered box represents a channel on a strip, depth, or grid electrode. Adjacent pairs of channels were subtracted from each other. Top: Referencing scheme for strip or depth electrodes. Bottom: Referencing scheme for grids.

2.5 Automatic HFA Detector

Automatic detection is crucial for any study involving HFAs, and the criteria selected by different investigators for automatic detectors are varied (Worrell et al., 2012). Generally, EEG is first band-pass filtered; then, an energy threshold is computed; segments of EEG statistically larger than threshold for a minimum duration are considered possible HFAs (Worrell et al., 2012; Zelmann et al., 2012). The main difference among the detectors is the type of energy function computed on the filtered signal and the post-processing step to reject false detections.

The detector used in this study was a variant of one of the first automatic detectors published, which was based on the energy defined as the moving average of the root mean square (RMS) amplitude of a filtered signal (Staba et al., 2002). In this detector, each bipolar referenced signal was first band-pass filtered into two frequency bands: 80-250 Hz (ripple) and 250-500 Hz (fast ripple) using a finite impulse response filter. The root mean square (RMS) amplitude of the band-passed filtered signal was calculated using a 50 millisecond sliding window. This sliding window was advanced one data point at a time until the end of the signal was reached. Consecutive RMS values 3 standard deviations ($\boldsymbol{\sigma}_{\text{rms}}$) above the mean amplitude ($\boldsymbol{\mu}_{\text{rms}}$) of the background RMS signal were detected and delimited by onset and offset time markers as candidate HFAs. Consecutive events separated by less than 50 milliseconds were combined into one event.

In the original method developed by Staba et al. (2012), the RMS threshold was computed based on the entire signal, including the events. However, we found that this method failed in active channels. To improve performance, background sections –

segments without oscillatory components – were first detected, and the threshold was computed based on the values in the detected background.

To identify the background sections, the RMS signal for each channel was first cut into 100 millisecond segments. For each segment, three parameters were calculated: (1) α, the sum of the absolute differences of consecutive values; (2) β_{rms}, mean, and (3) γ_{rms}, standard deviation. The segments were ranked according to α, and the segments with the lowest 10% were considered as background segments. Segments with low α values indicated a very stable RMS and thus were likely to be part of the background signal, rather than the transient high frequency activity we were trying to detect. β_{rms} and γ_{rms} were then averaged to get $\boldsymbol{\mu}_{rms}$ and $\boldsymbol{\sigma}_{rms}$, respectively. The threshold was then set to $\boldsymbol{\mu}_{rms}$ plus 3 times $\boldsymbol{\sigma}_{rms}$.

As a post-processing step, candidate HFAs were required to have a minimum of 6 peaks greater than 5 SD ($\boldsymbol{\sigma}_{rectified}$) above the mean rectified band-passed signal ($\boldsymbol{\mu}_{rectified}$) of the background segments. To calculate $\boldsymbol{\mu}_{rectified}$ and $\boldsymbol{\sigma}_{rectified}$, the mean ($\beta_{rectified}$) and SD ($\gamma_{rectified}$) of the absolute value of the band-pass filtered signal of previously identified background segments were averaged, respectively.

Events that satisfied all the mentioned criteria in the 80-250 Hz and 250-500 Hz band-passed filtered signal were identified as ripples and fast ripples, respectively. Figures 4-7 illustrate each step in detecting ripples from a 2 second segment of data.

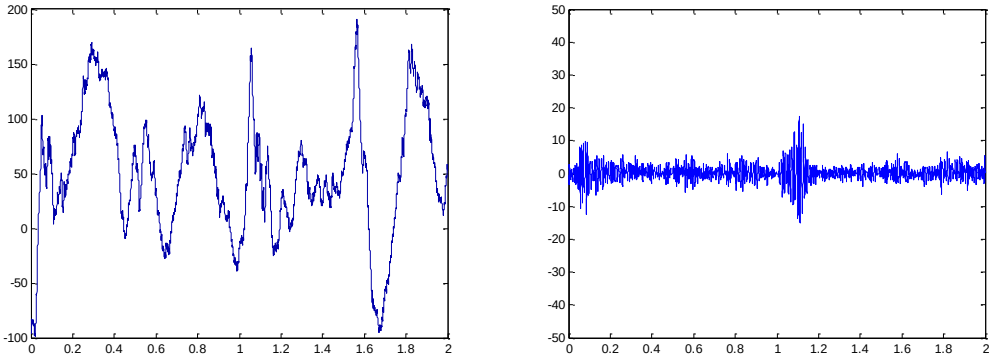

Figure 4. Band-pass filtering of data. Left – bipolar referenced signal. Right – 80-250 Hz band-passed filtered signal.

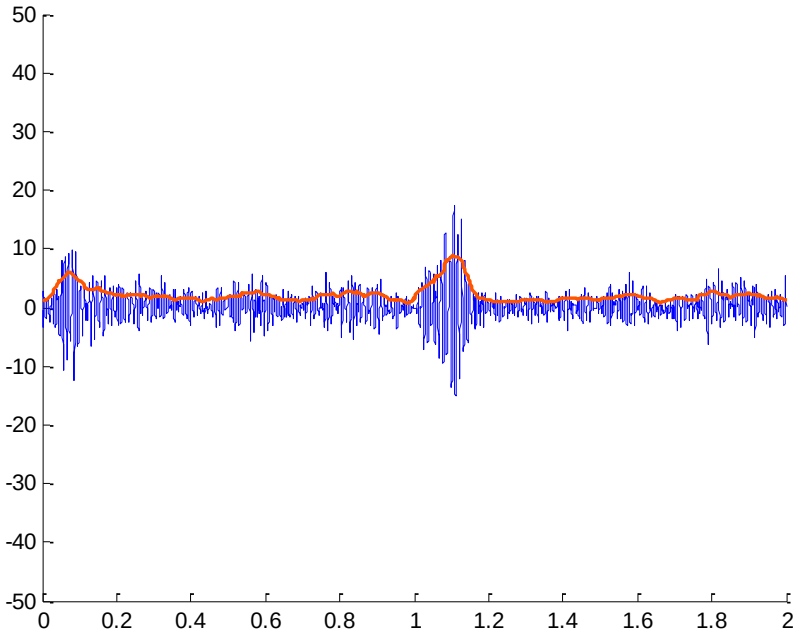

Figure 5. Moving average of the root mean square amplitude. RMS values superimposed on 80-250 Hz band-passed filtered signal.

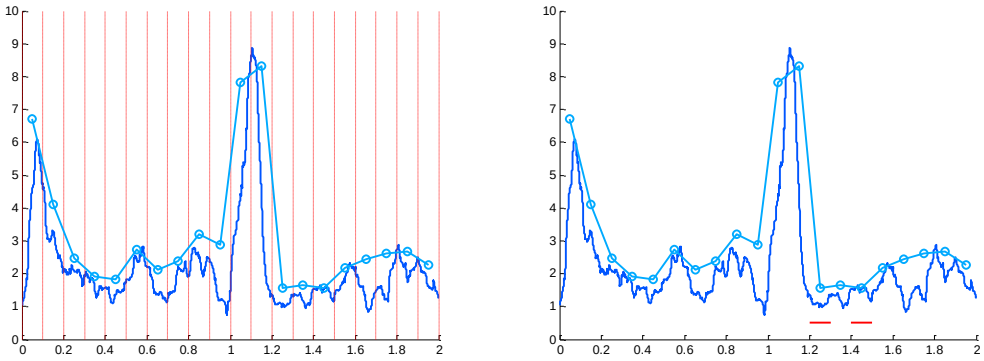

Figure 6. Background detection. Left: α values (light blue circles) superimposed on the RMS signal (dark blue line). Dashed lines indicate start and end of each segment. Right: Identified background segments marked by red horizontal lines.

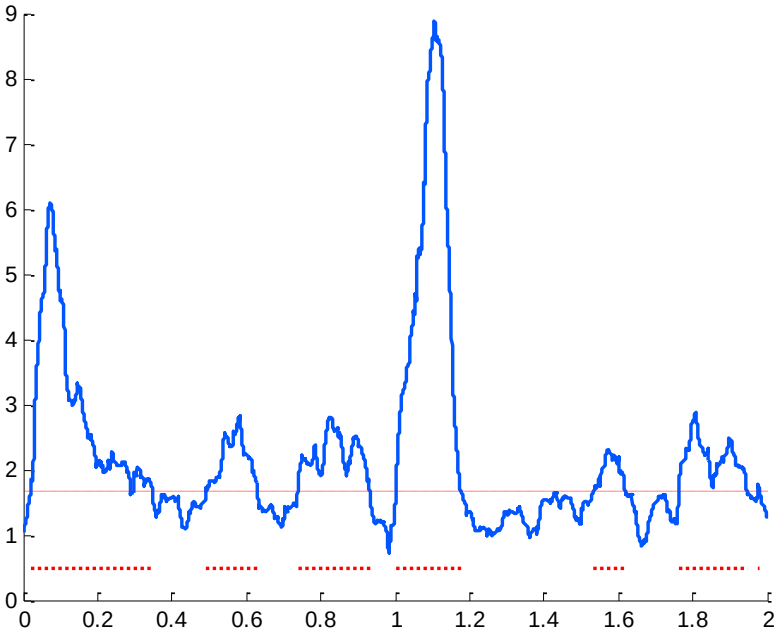

Figure 7. Initial detection of segments above the threshold. RMS values above threshold (red dashed line) identified by red dotted lines.

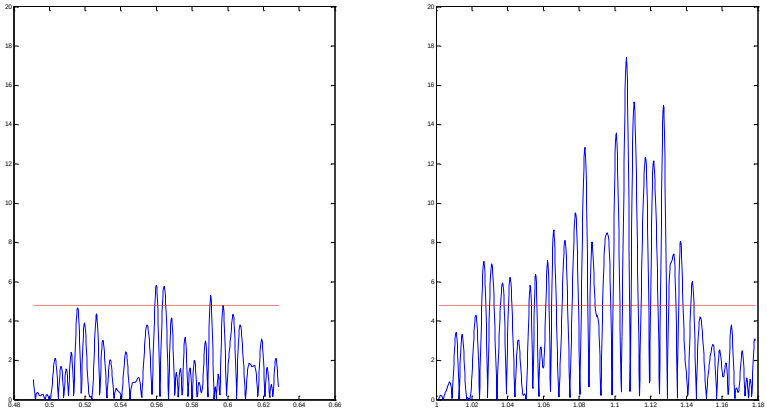

Figure 8. Post-processing. Number of peaks above threshold requirement. Both panels show the rectified-band-passed signal of the 2nd (left) and 4th (right) candidate ripples marked in figure 7. The candidate ripple shown on the left was rejected because it only had 3 peaks above threshold (horizontal dashed line)

2.6 Visual Identification of HFAs

High-frequency activity were visually identified for validation and optimization of our automatic detector. The first two minutes of intracranial EEG data from four sites across three patients were reviewed and marked for HFAs. The visual identification method was similar to the one implemented to identify HFAs in human interictal recordings (Jacobs et al., 2008). During visual marking of HFAs, channels were displayed at a time resolution of 0.6 s (3000 data points of a signal sampled at 5000 Hz) across a computer monitor. The signal was high-pass filtered at 80 and 250 Hz using a finite impulse response filter. The display was split vertically into three panels — an 80 Hz high-pass filter, a 250 Hz filter high-pass filter, and a third panel containing the analytical amplitude of each filtered signal placed on top of each other (Figure 9). This amplitude was calculated by using the Hilbert transform of the band-passed filtered signal.

A ripple was marked if an event clearly stood out of the background on the side of the 80 Hz filter and did not show the same shape on the side of the 250 Hz filter. An event was regarded as a fast ripple if it was only visible in the 250 Hz filter. If ripples and fast ripples occurred at the same time, they had to have different shapes to be regarded as separate events (Jacobs et al., 2008).

The visually marked HFAs were considered the gold standard, and the detector parameters were optimized based on this standard.

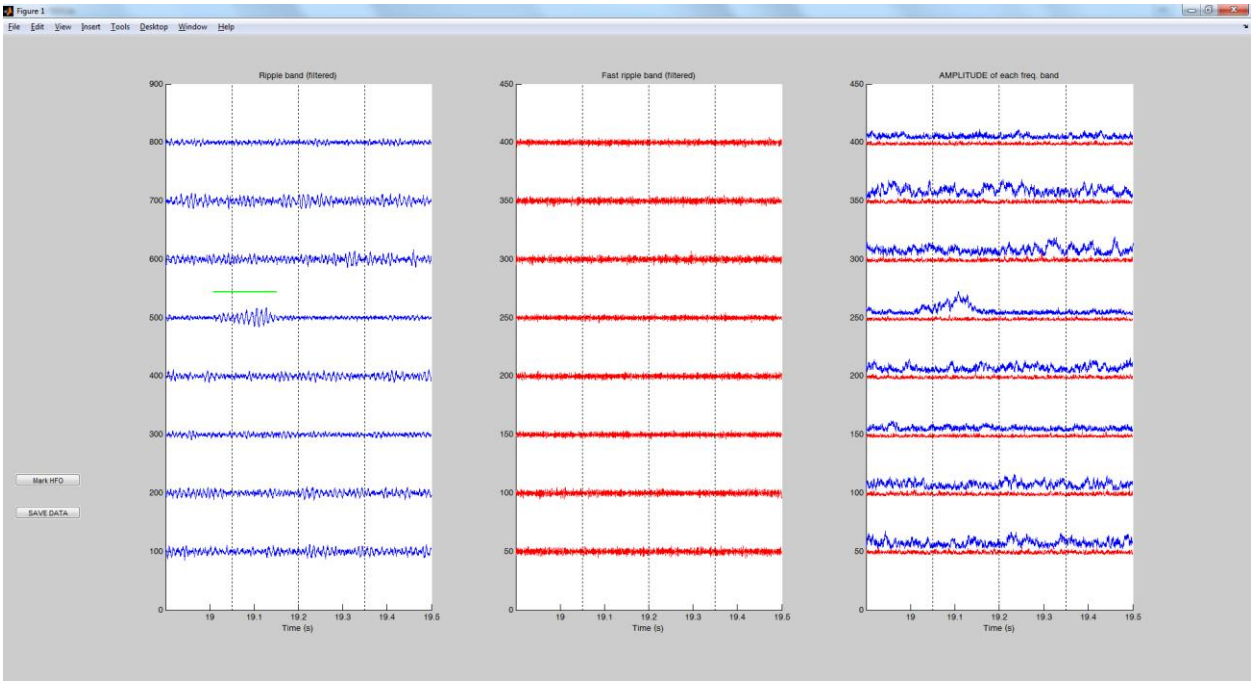

Figure 9. Panel for visual marking of HFAs. Left Panel: ripple band. Middle Panel: fast ripple band. Right Panel: amplitude for ripple band (blue), –and amplitude for fast ripple band (red). An example of a marked ripple HFA is shown under the green line on the left panel.

2.7 HFA Detector Optimization

Automatic detection requires a high specificity and sensitivity to be useful. To improve performance, the detector's parameters were optimized to best detect the visually marked ripples from the test data (Table 2). By defining HFAs as spontaneous

events that were distinguished from ongoing background activity, the statistical relationship of ripples to the 80-250 Hz background was similar to that of the fast ripples to the 250-500 Hz background. Therefore, the parameters optimized for ripple detection carried over to fast ripple detection. This seems to be standard practice, as implemented by several research groups (Staba et al., 2002; Gardner et al., 2007; Crepon et al., 2010; Zelmann et al., 2012).

Table 2. List of optimized detector parameters and their description.

Parameter		Description	Tested Values	Optimized Values
Initial Detection	Sliding window (ms)	Length of window to calculate the moving average of the root mean square amplitude	10, 25, 50	50
	RMS threshold (SD)	number of SD above RMS baseline	3, 4, 5	3
	Segment length for baseline calculation (ms)	Length of each segment into which the entire RMS signal was divided into	100, 250, 500	100
	RMS baseline percentage (%)	Lowest % of α values to identify background segments.	10, 20, 50	10
	Minimum HFA duration (ms)	Length of consecutive RMS above threshold	10, 50, 100	10
Post-Processing	Threshold for HFA peaks (SD)	number of SD above rectified baseline	3, 4, 5	5

	Minimum peaks above threshold	number of peaks above rectified baseline threshold	3, 4, 6	6

To observe the effect of each parameter in the detector's ability to detect the visually marked ripples, the detector was run with a set of parameters on a two minute data while adjusting one parameter at a time (Figure 10-16). However, in reality, some of the parameters are coupled. For example, increasing the window length for the moving RMS calculations will decrease the RMS standard deviation; thus, decreasing the threshold. Adjusting the parameters one at a time provides an overall understanding on the role each plays in the detector performance. Moreover, this process allowed us to constrain the choices for each parameter to three which resulted in a total possible 2178 (3^7) parameter combinations and ultimately saving computation time (Figure 17). These values were chosen based on maintaining a high number of true positives while minimizing the number of false detections (Figure 18).

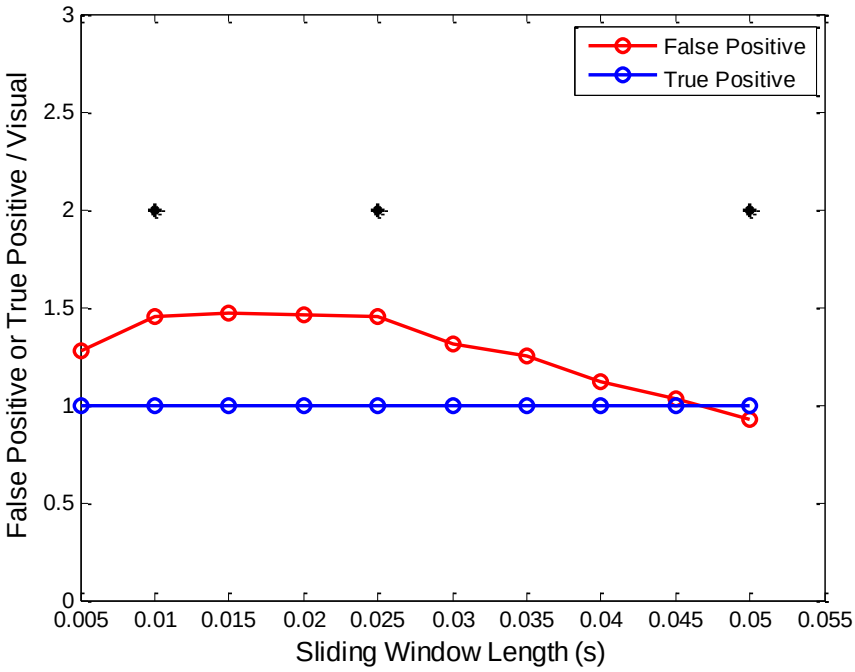

Figure 10. Sliding Window Length. A longer sliding window smoothed the RMS signal more and thus resulted in fewer total detections. This parameter did not have an effect on the number of true positives. Black asterisks indicate chosen values for optimization.

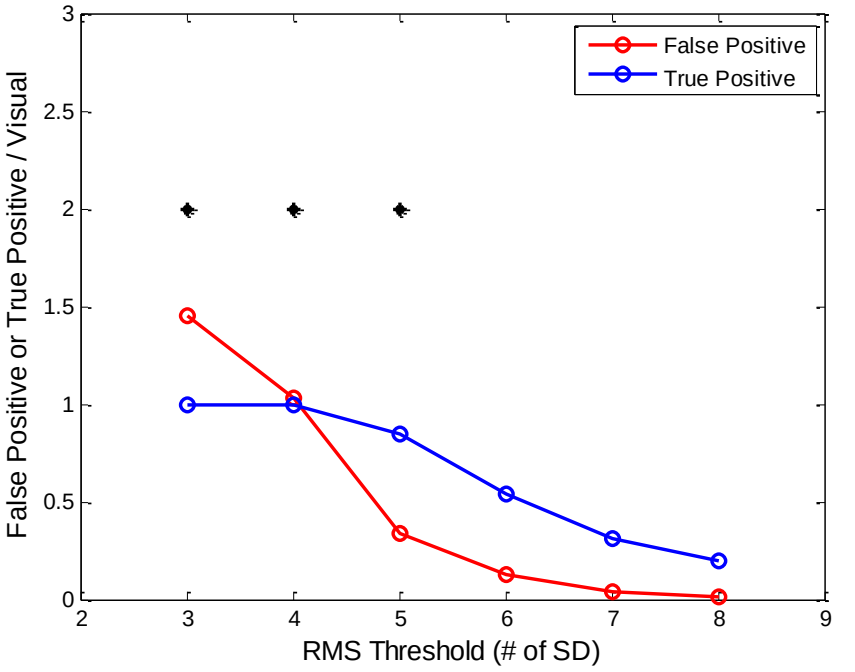

Figure 11. RMS threshold. Increasing this parameter resulted in a more strict criteria, thus reducing the total number of detections. Black asterisks indicate chosen values for optimization.

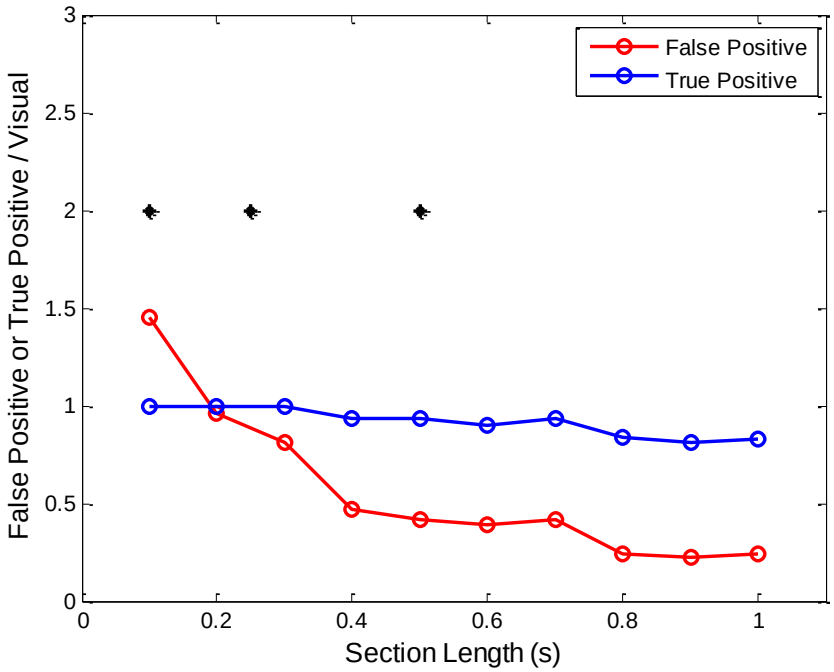

Figure 12. Segment Length. The segment length barely changed the number of true positives, but it reduced the number of false positives. This was expected since increasing the segment length would increase the threshold. Black asterisks indicate chosen values for optimization.

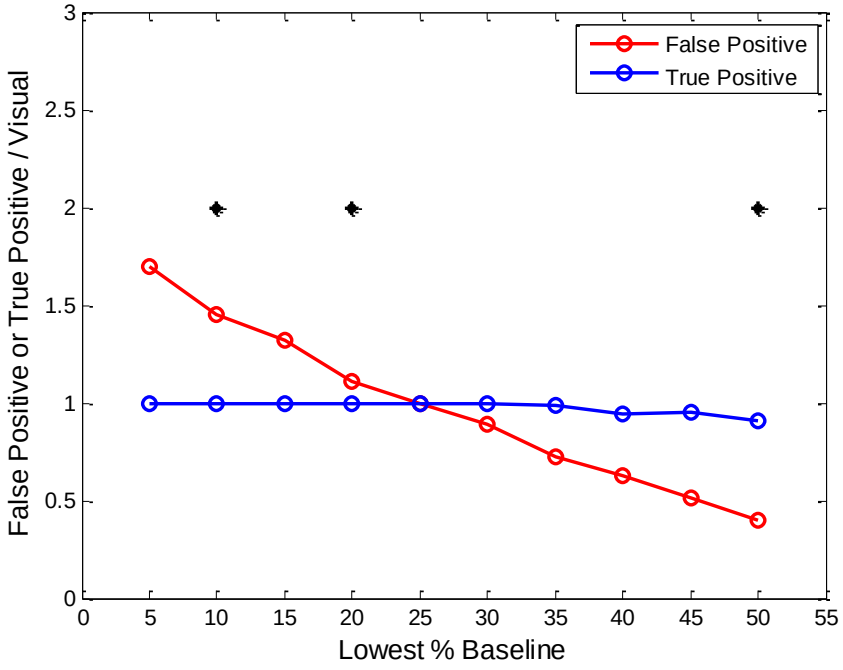

Figure 13. RMS baseline percentage. The percentage baseline barely changed the number of true positives, but it reduced the number of false positives. This was

expected since increasing the percentage baseline would increase the threshold. Black asterisks indicate chosen values for optimization.

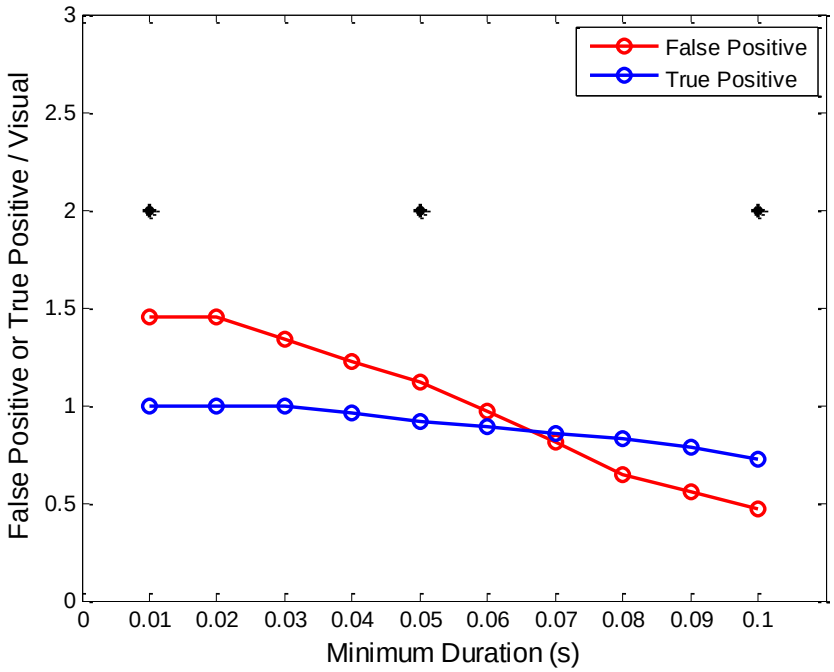

Figure 14. Minimum duration. Increasing the minimum duration reduced the number of false positives more than true positives. Black asterisks indicate chosen values for optimization.

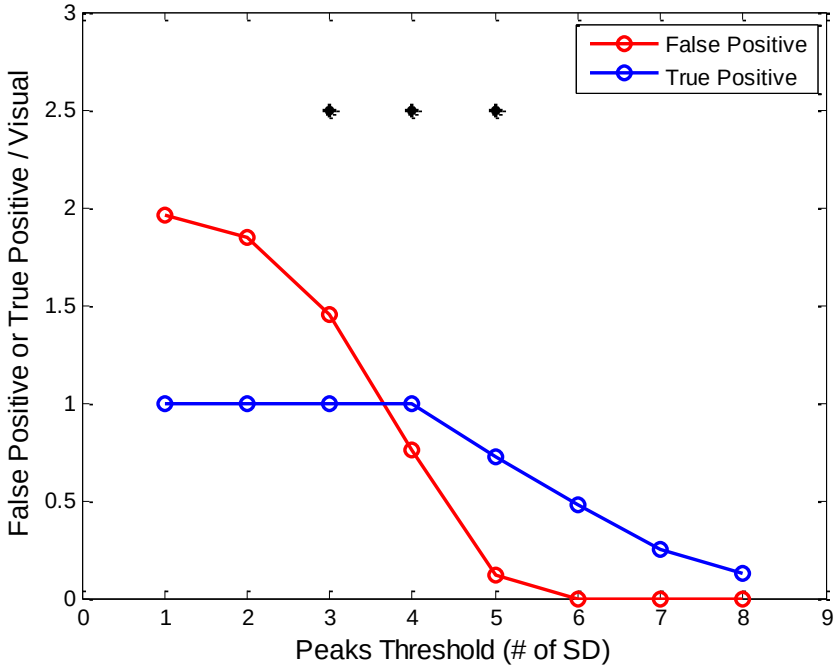

Figure 15. Rectified band-pass threshold. Increasing the threshold reduced the total number of detections. However, the number of true positives was unaffected until the value went above 4 SD. Black asterisks indicate chosen values for optimization.

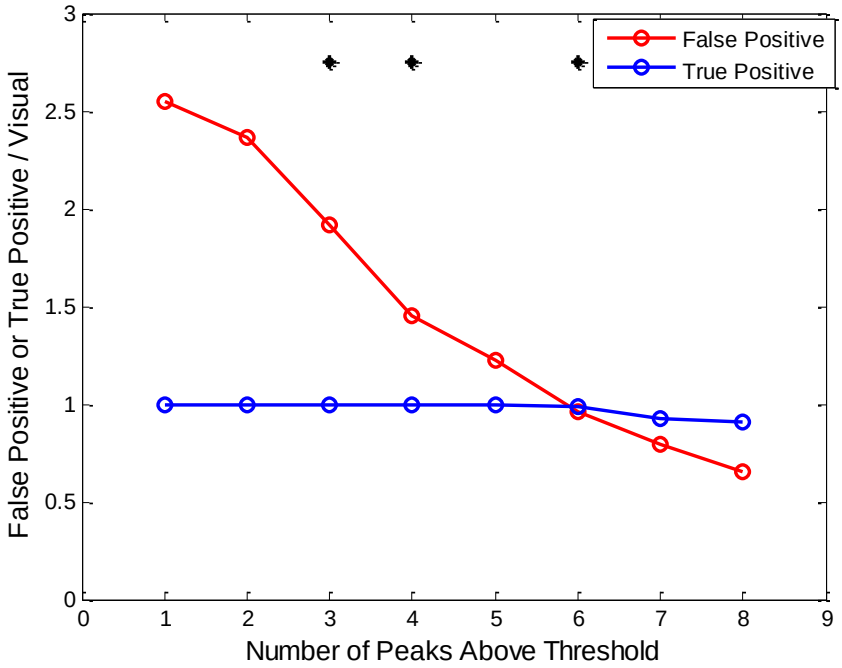

Figure 16. Minimum peaks. Increasing the peak requirement did not affect the number of true positives, but it reduced the number of false positives. Black asterisks indicate chosen values for optimization.

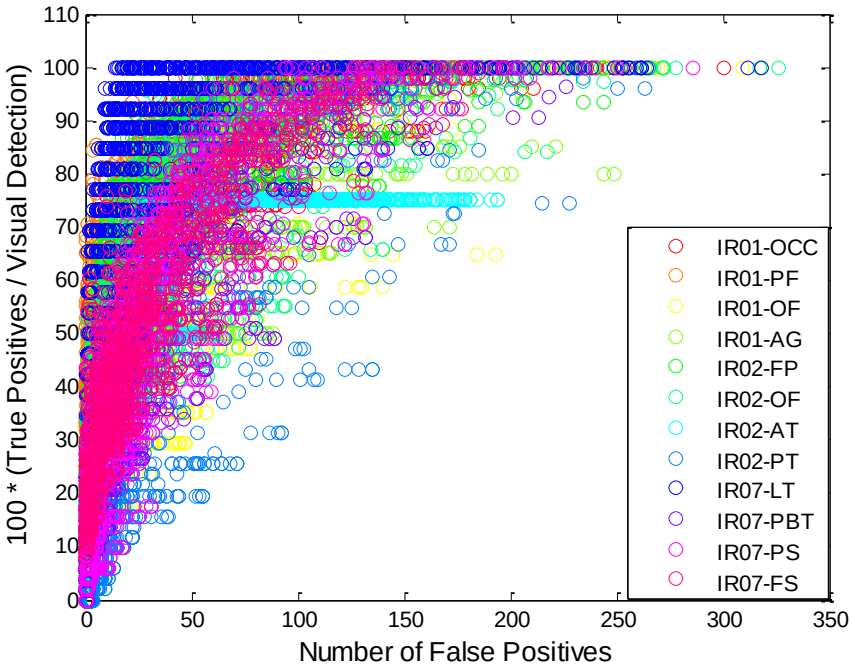

Figure 17. Detector performance on test data. Each circle represents a set of parameters for a given run on test data. Each color represents a Patient / Location Combination. OCC: occipital; F: frontal; OF: orbitofrontal; T: temporal; A: anterior; P: posterior; L: Left; S: strip; G: grid. All nomenclature was determined based on the approximate location and presence of other electrodes implanted in each patient.

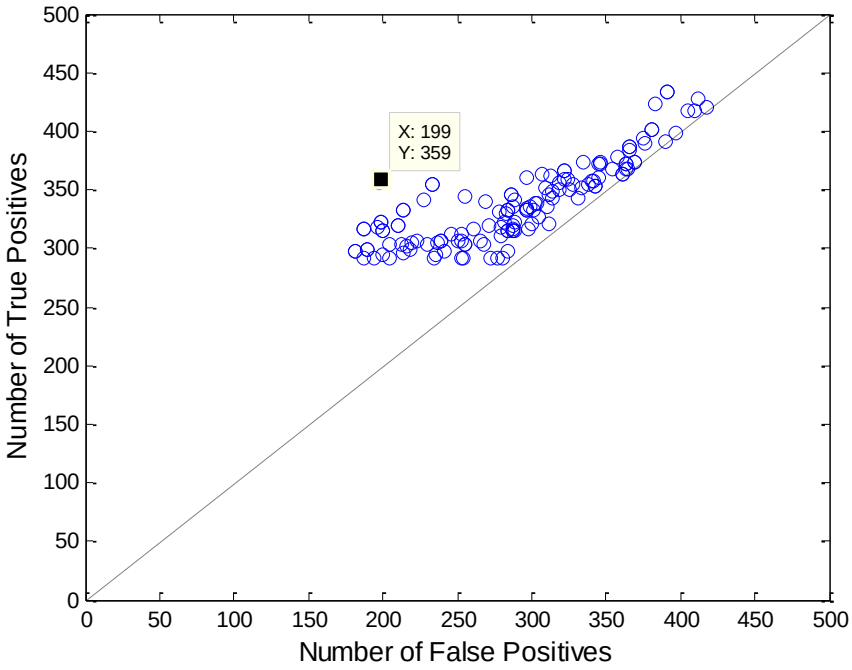

Figure 18. Choosing detector parameters. Results from parameter sets that detected at least 50% of the visually marked ripples and that had a greater number of true positives than false positives across all twelve channels of test data. The labeled point indicates the number of false positives (199) and true positives (359) using the optimized parameter values listed in Table 2.

The results from all patient/site combination were aggregated (Figure 17). A total of 581 ripples with unequal distribution across patient/site were visually identified in the test data. The parameters used for the rest of the study were the set that yielded the highest ratio of true positives with respect to false positives and that detected at least 50% of the total visually marked ripples across all twelve test datasets (Figure 18; Table 2).

2.8 HFA characteristics

The number of ripples and fast ripples were compared between landscapes or fearful faces. Furthermore, the Z-score of the RMS signal, peak frequency, and duration were compared between the two conditions at the locations where the rate was significantly different.

To calculate the Z-score of each detected HFA, the RMS signal delimited by the onset and offset was averaged. The $\boldsymbol{\mu}_{\text{rms}}$ was then subtracted from this value, and the difference was divided by the $\boldsymbol{\sigma}_{\text{rms}}$.

To determine the peak frequency of each detected HFA, the HFA candidate was extended 50 ms at both sides, zero padded to the nearest next power of 2, then the Fast-Fourier Transform of the band-pass filtered signal was taken. The frequency at which the maximum power occurred was then set as the peak frequency of the HFA.

HFA Duration was calculated by subtracting the onset and offset times.

2.9 Statistical Analysis

The study tested for differences in the number of HFAs between the eight baseline and eight activation blocks across all 465 bipolar signals. P-values were computed using the Mann-Whitney U test for every bipolar signal, and the significance level was determined by the Benjamin-Hochberg procedure with a false discovery rate of 0.2.

At the sites with significant differences in the number of HFAs, the amplitude, frequency, and duration between HFAs found in the baseline blocks versus the HFAs found in the activation blocks were compared using Mann-Whitney U test ($p<0.0167$, corrected for three comparisons).

Furthermore, the mean number of HFAs in the first 12 seconds of a block was compared to the last 12 seconds to determine whether the transition between blocks generated a significantly higher rate of HFAs than the ongoing presentation of faces or landscapes.

3 Results

3.1 HFA Detection

A total of 55,776 HFAs (Ripples: 43,480) were detected from 465 non-SOZ sites with 384 seconds of data from each site. Across all electrode locations, 51% of ripples were detected during activation. Fifty one percent of fast ripples (6,234) were also detected during activation (Figure 19). The mean rate of ripples was 14.6 per minute while the mean for fast ripples was 4.1 per minute.

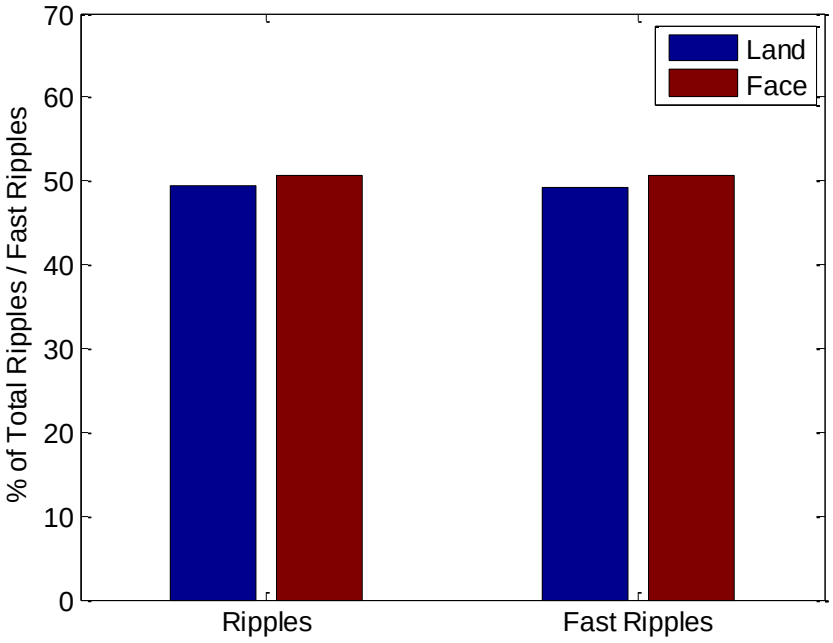

Figure 19. Distribution of ripples and fast ripples across landscape (baseline) blocks and fearful face (activation) blocks in non-SOZ channels.

3.2 HFAs in Face Processing Regions

We found 18 sites where there was a significant difference in the number of ripples when comparing landscape blocks and face blocks. The number for faces was significantly greater than landscape in 14 out of the 18 ($p<0.008$, Mann-Whitney U test, corrected for multiple comparisons via Benjamini-Hochberg procedure). Among the 14

sites, the average number of ripples found in face blocks was 13.5 ± 5.5 (± SD) compared to 7.8 ± 5.7 for land blocks. The 14 sites were spread across four different patients (Figure 20) and were located on the frontal lobe (8), temporal lobe (4), and occipital lobe (2). The four sites where landscape (10.9 ± 5.1) was significantly greater than faces (5.1 ± 3.6) were located in the frontal (1), orbitofrontal (1), and temporal (2) regions.

For fast ripples, only 1 site showed significantly greater in faces than landscape ($p<0.0004$, Mann-Whitney U test, corrected for multiple comparisons via Benjamini-Hochberg procedure). The mean number of fast ripples found in face blocks was 11.4 ± 2.6 while the average for landscape blocks was 2.1 ± 1.5.

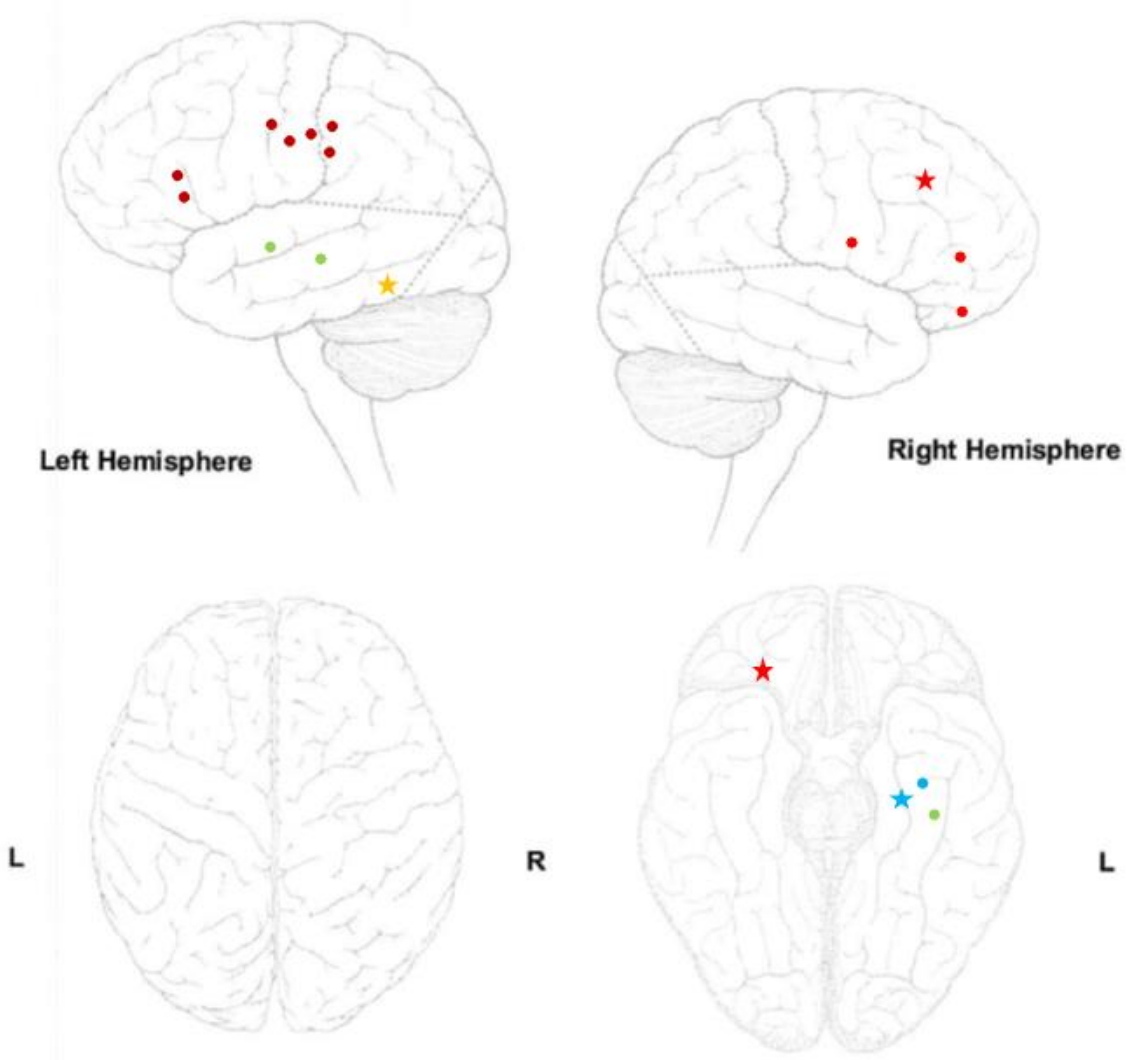

Figure 20. Approximate location of sites with significant differences in HFA rates. Circles indicate sites where the number of ripples in faces are significantly greater than the number in landscape, while stars indicate the opposite ($p<0.008$). Different colors represent different patients. The lone site where the number of fast ripples in faces was significantly greater than the number in landscapes is also indicated by the green circle on the bottom right diagram.

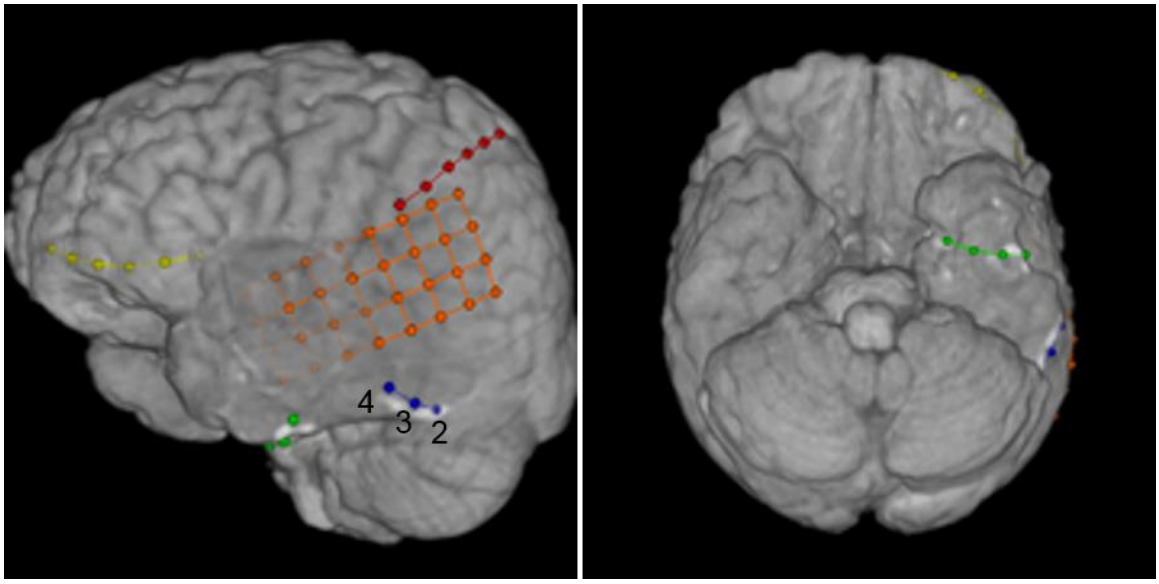

Figure 21. Co-registered images for Patient 7 showing 1 x 4 strip electrode on basal temporal region (blue). The number of ripples and fast ripples were both significantly greater during face blocks than during landscape blocks in the bipolar referenced signal 1-2 (1 not shown, but adjacent to 2). This site corresponds to the green circle in the basal temporal region in figure 20.

The increase in HFA rates during fearful face viewing were evident on a block-by-block basis across the 14 sites. To illustrate this phenomenon, the HFA activity (Figure 22) from a four channel electrode placed on the temporal lobe of patient 7 is shown (Figure 21). PBT1 – PBT2 represents the bipolar referenced signal recorded from channels 1 and 2, while PB3 – PBT4 is the bipolar referenced signal for channels 3 and 4. The number of ripples and fast ripples in PBT1 – PBT2, indicated by the blue and red circles respectively, increased when the patient was viewing fearful faces and decreased during landscape viewing. This behavior was not observed in the adjacent PB3 – PBT4. The sum of HFAs for each block is shown in figure 22 (middle), while the total across all blocks along the signal is compared in figure 22 (bottom). For PBT1-2, the average number of ripples was 16 ± 2.6 in face blocks while the average for landscape blocks was 5 ± 2.0. In contrast, the average number of ripples in PBT3-4 was 4.6 ± 1.8 for face blocks while it was 5.1 ± 2.4 for landscape blocks.

3.3 HFAs in non-face processing regions

There were also sites where the HFA rates increased during landscape viewing compared to fearful face viewing. Figure 23 shows the rate of HFAs for another pair of adjacent sites, this time from a basal temporal strip implanted in patient 8. These sites correspond to the blue star (PST1-PST2) and circle (PST3-PST4) marked at the bottom right diagram of figure 20. In PST1-PST2, the landscape blocks (8.6 ± 3.6) had significantly greater number of ripples than the face blocks (2.3 ± 1.7). On the other hand, the opposite was observed at the adjacent site PST3-PST4, where the faces (6.9 ± 2.5) were significantly greater than the landscape (3.0 ± 2.1).

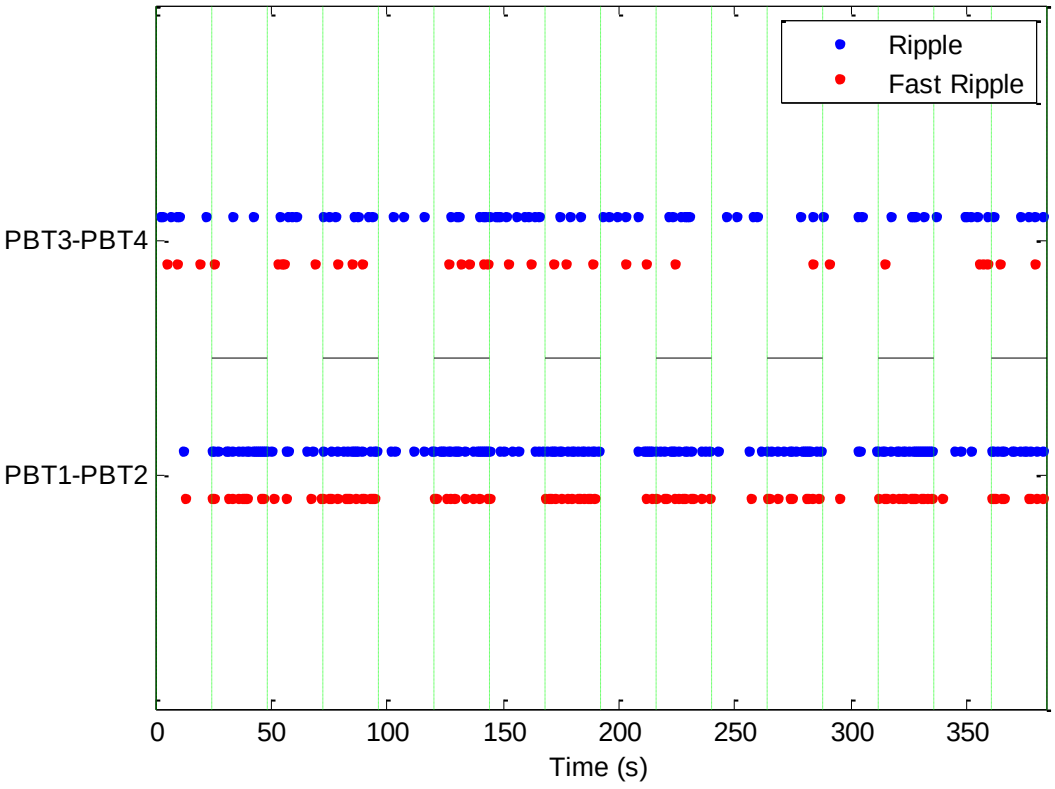

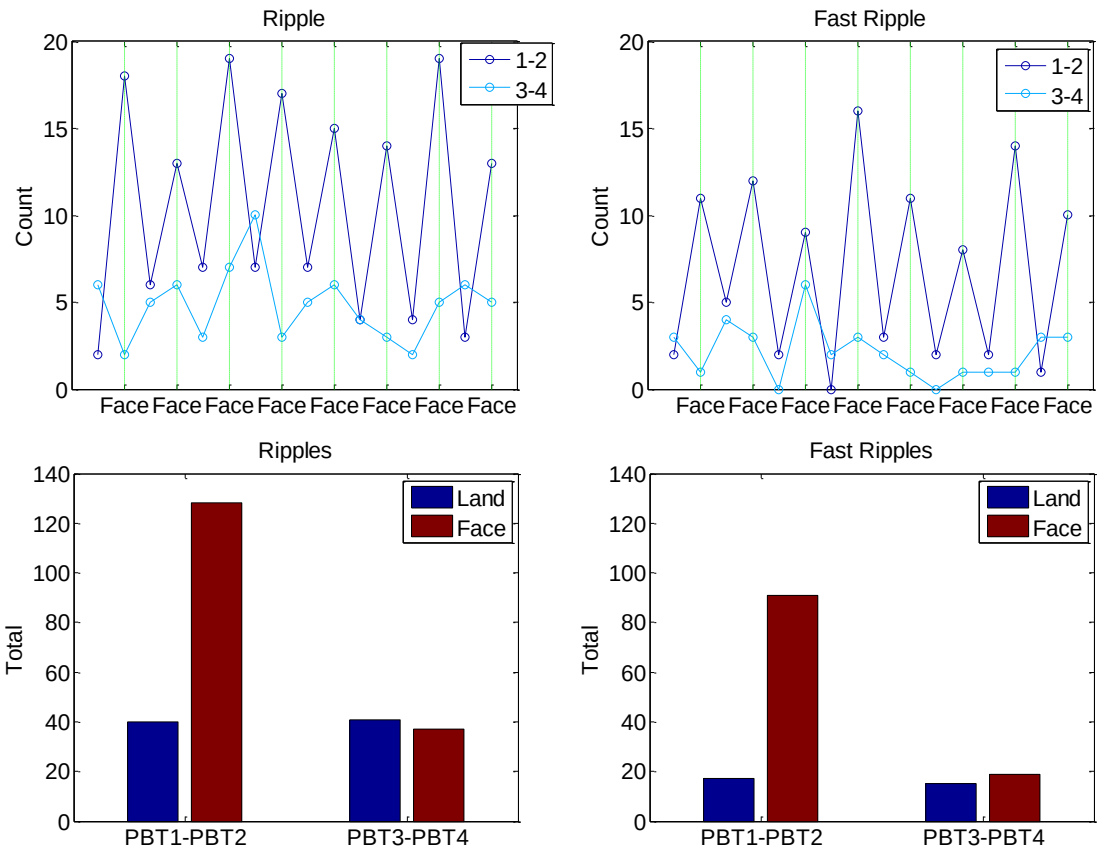

Figure 22. HFAs in face processing regions. Top: Start times of HFAs along the bipolar referenced signals from electrodes illustrated in figure 21. Green vertical lines indicate transitions between baseline and activation. Black horizontal lines indicate activation (face) blocks. PBT: Posterior basal temporal. Middle: Number of HFAs (Left: Ripple, Right: Fast Ripple) per block for the sites shown in Figure 21. Bottom: Total HFAs across all blocks (Left: Ripple, Right: Fast Ripple).

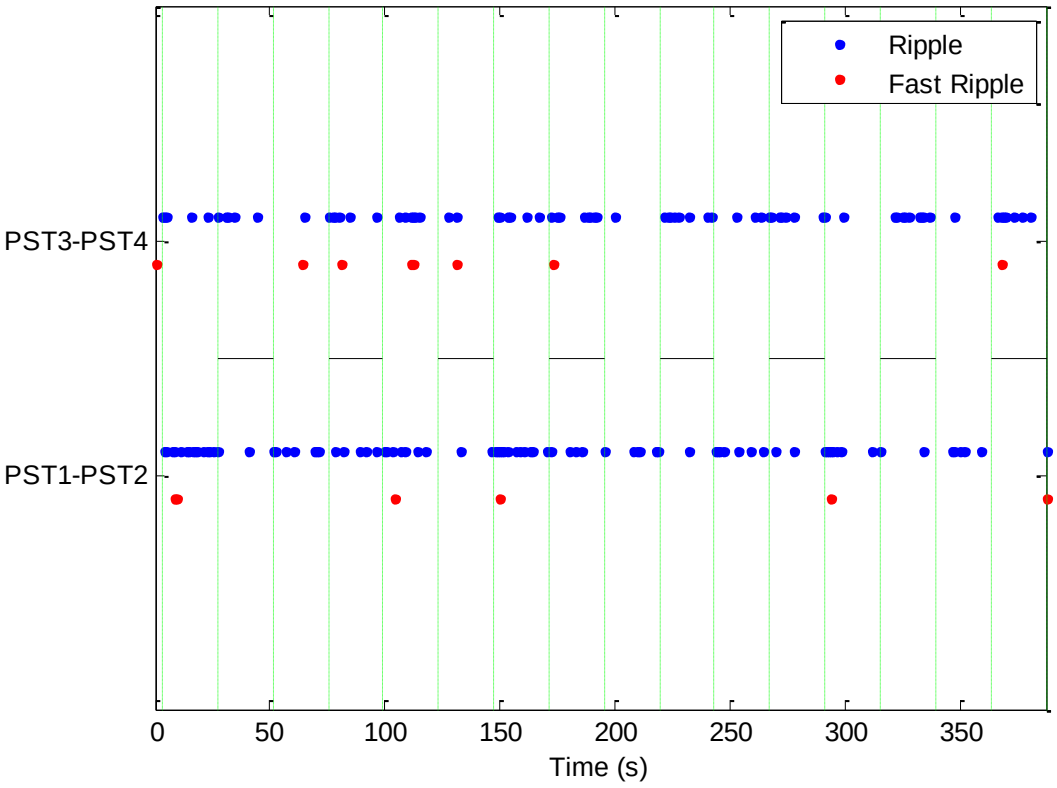
Ripple
Fast Ripple
PST3-PST4
PST1-PST2
0
50
100
150
200
250
300
350
Time (s)

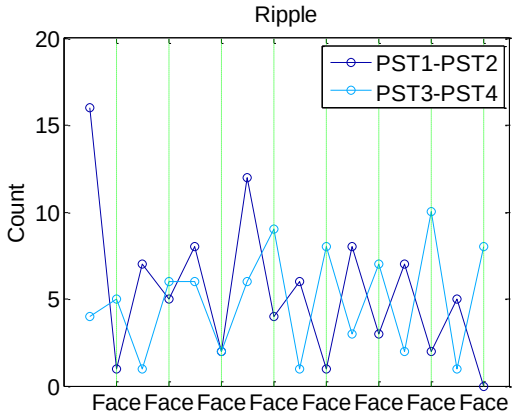
Ripple
PST1-PST2
PST3-PST4
Count
20
15
10
5
0
Face Face Face Face Face Face Face Face

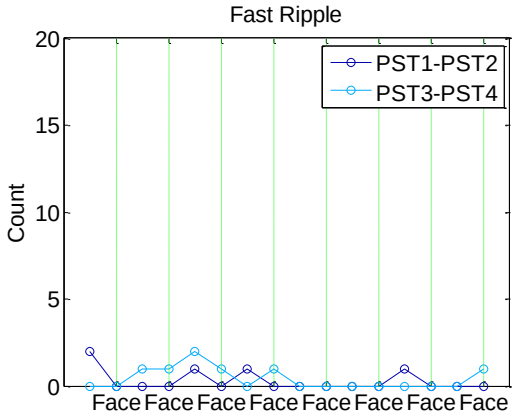
Fast Ripple
PST1-PST2
PST3-PST4
Count
20
15
10
5
0
Face Face Face Face Face Face Face Face

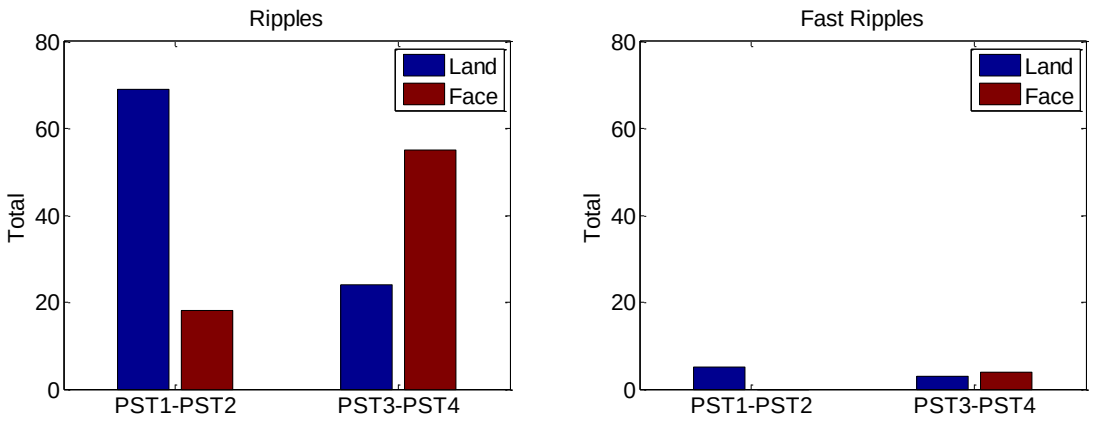

Figure 23. Adjacent face and land processing regions. HFAs rates for the blue star (PST1 – PST2) and circle (PST3 – PST4) sites indicated in the basal temporal region in figure 20.

3.4 HFA Characteristics

The frequency, amplitude, and duration of HFAs were also compared across the landscape and face blocks in sites where the HFA rates were significantly different (Table 3). The average values for sites identified as part of the seizure-onset-zone are also included here for comparison. Note that the HFAs were not categorized as face or landscape in calculating the average values for the SOZ sites.

The average peak frequency for ripples found during face blocks (94.9 ± 6.6) was slightly higher than the average for HFAs during landscape blocks (94.1 ± 6.6) ($p<0.02$, MWU test, corrected for three comparisons). On the other hand, the frequency for fast ripples found during face blocks (276.0 ± 18.1) were slightly higher than the ones found during landscape blocks (270.2 ± 11.6), but these were not found to be statistically significant.

There were no significant differences in the amplitude Z-score in both ripples (land: 7.7 ± 4.2; face: 7.7 ± 3.1) and fast ripples (land: 4.8 ± 1.4; face: 5.1 ± 0.6) between landscape and faces.

Moreover, there were also no significant differences in the duration in both ripples (land: 606 ± 38 milliseconds; face: 588 ± 38 ms) and fast ripples (land: 545 ± 30 ms; face: 549 ± 26 ms) between landscape and faces.

Furthermore, the HFAs from SOZ onset zone were also characterized. Across the 129 bipolar signals categorized as SOZ, 22,104 HFAs (ripples: 15,318) were detected. 49% and 51% of ripples and fast ripples, respectively, were found during landscape blocks. No individual SOZ sites were found to have significant differences in HFA rates across landscape and faces. The mean rate of ripples in the SOZ sites was 18.6 per minute and the mean rate of fast ripples was 8.2 per minute.

Table 3. HFA characteristics.

	Landscape	Face	SOZ sites
Frequency (Hz)			
Ripples	*94.1 ± 6.6	*94.9 ± 6.6	100.2 ± 24.0
Fast Ripples	270.2 ± 11.6	276.0 ± 18.1	294.4 ± 44.8
Amplitude (Z-score)			
Ripples	7.7 ± 4.2	7.7 ± 3.1	11.9 ± 13.9
Fast Ripples	4.8 ± 1.4	5.1 ± 0.6	12.2 ± 22.2
Duration (ms)			
Ripples	606 ± 38	588 ± 38	553 ± 1416
Fast Ripples	545 ± 30	549 ± 26	488 ± 4214

*p<0.02. Mean ± SD.

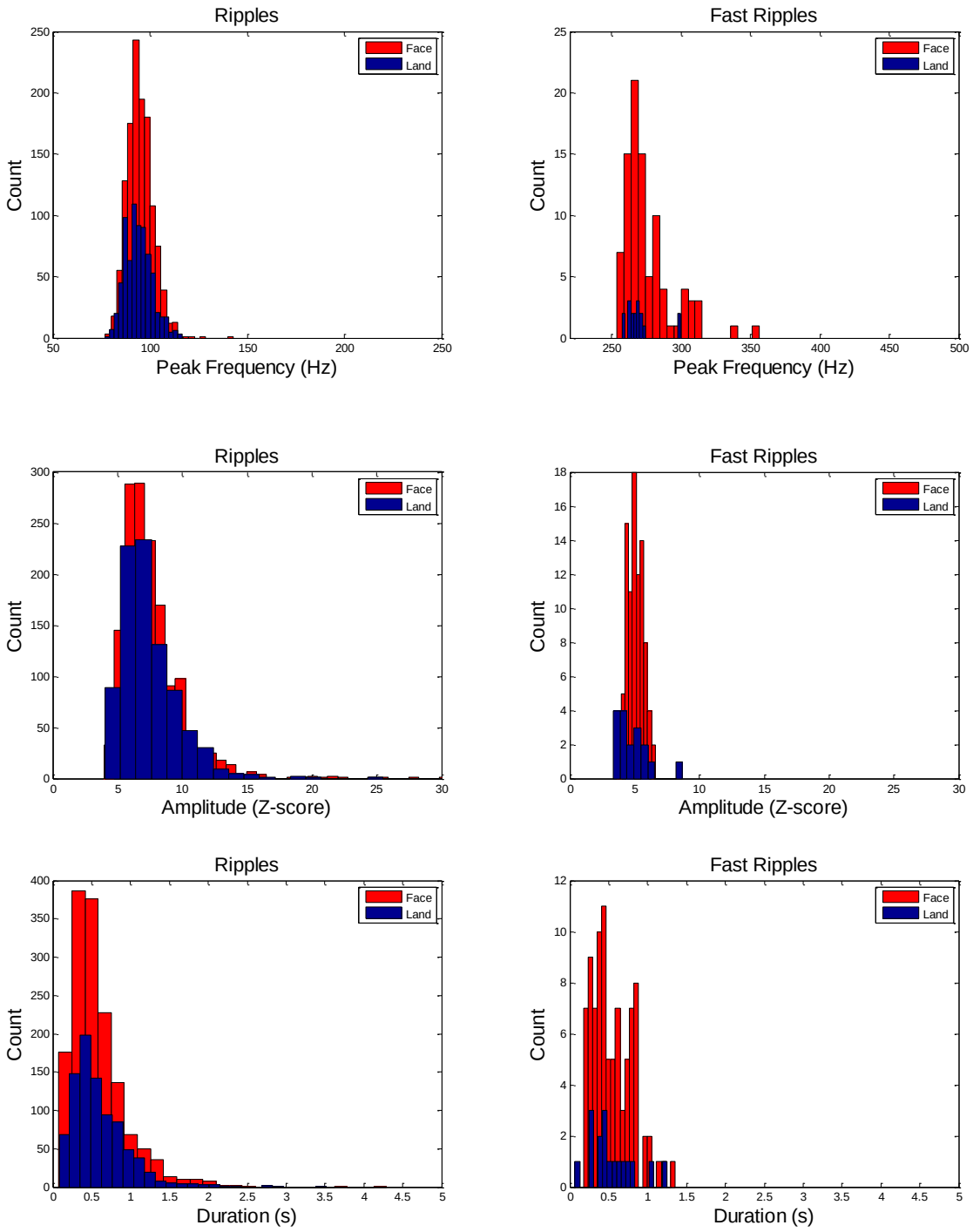

Figure 24. HFA characteristics in landscape and face blocks. Histograms of peak frequency (top), amplitude (middle), and duration (bottom) of detected ripples (left) and fast ripples (right) found in baseline (blue, landscape) and activation (red, face). Results are from channels in which HFA rate was significantly different for face and landscape blocks.

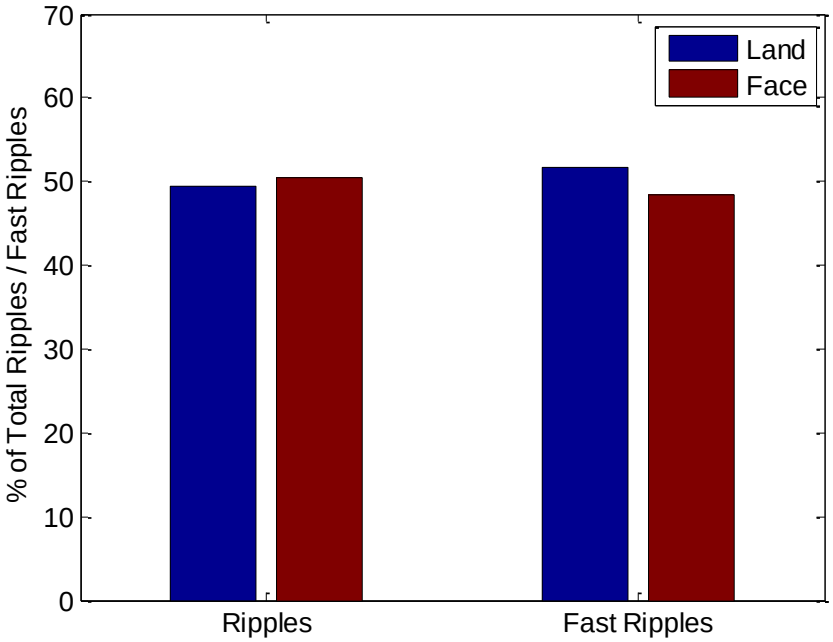

Figure 25. Distribution of ripples and fast ripples across landscape (baseline) blocks and fearful face (activation) blocks in SOZ channels.

3.5 HFA response over time

Table 4 compares the average number of HFAs found during the first 12 seconds to the last 12 seconds of each block among the sites with significant differences. In other words, for the sites (14 for ripples, 1 for fast ripples) where faces were significantly greater than landscape, the number of HFAs found during the first twelve seconds was compared to the number found during the last twelve seconds of each face block. This test was done to check whether the significant differences in landscape versus faces are due to a large number at the transition point between the two conditions. No significant differences were found for both ripples and fast ripples. Similarly, the first and second half of landscape blocks were compared among the four sites where the landscape was significantly greater than faces. Again, no significant differences were found between the first and second half of each block.

Table 4. Comparison of first and second half of each block.

	Landscape		Face	
	First Half	Second Half	First Half	Second Half
Ripples	6.1 ± 2.9	4.8 ± 3.0	6.8 ± 3.2	6.7 ± 3.1
Fast Ripples	-	-	5.5 ± 1.3	5.9 ± 1.5

4 Discussion

We have shown that ripples and fast ripples were evoked in several brain regions when subjects were presented with fearful face stimuli. Furthermore, in certain locations, the effect was strong that the change of HFA rates were visually apparent on a block-to-block basis (Figure 22). These sites were spread across the temporal sulcus, ventral temporal, and parietal regions – regions previously implicated in face processing in normal and epileptic brain (Haxby et al., 2000; Engel and McCarthy, 2011; Collins and Olson 2014; Riley et al., 2015). Increased HFA rates were also observed in the frontal region, where face-processing nodes have not been previously found. However, this was observed in only one patient. These results were unique from previous investigations in that the rate of transient high frequency activity was used to characterize the face-processing regions, as opposed to the signal averaging approach used in ERP studies. Moreover, these results may be a step towards understanding the sensitivity of a brain region to task manipulations that is not evident in phased-locked ERPs.

The regions where there was significant difference across HFA rates were highly localized. Using a bipolar montage allowed us to localize the signal from just the two adjacent electrodes, leading to a high spatial resolution. The number of HFA over all the available sites across patients were distributed evenly (Figure 19). Only when we narrowed our analysis to individual bipolar signals when we saw significant differences across regions. Four out of the 18 sites showed significantly increased HFA during landscape viewing. One of these sites was even adjacent to a face-processing site. Indeed, this has been shown previously, where regions that responded more to either

faces or inanimate objects were next to each other (Haxby et al., 1999; Engel and McCarthy 2011; Weiner and Grill-Spector 2013). In addition, Epstein and Kanwisher named the ‘parahippocampal place area’ (PPA), a particular area within the human parahippocampal cortex that responds selectively and automatically in fMRI to passively viewed scenes, but only weakly to single objects and not at all to faces (1998). These results add further evidence that transient high frequency activity in the ripple and fast ripple band is not only specific to face-processing but could also be an index of cortical processing in regions that is involved by a task.

Automatic detection of high frequency activity is crucial. Our study used an automatic detector with the objective of detecting spontaneous events that can be distinguished from ongoing background activity. Since a standard general has not been established, we had to train and validate the detector with our dataset to obtain good performance (Worrell et al., 2012). To validate our detector, we measured its ability to successfully identify visually marked HFAs from a training set taken from our overall data. We followed guidelines from a previous study identifying HFOs in human interictal recordings (Jacobs et al., 2008). However, it should be noted that the performance was measured based on the visually marked HFAs in the ripple band only, as fast ripples were rare and difficult to identify visually. Nevertheless, since our detector identifies transient oscillations that are statistically greater than the baseline segments, the parameters should carry over to the detection of transient oscillations in the fast ripple band. This practice of having the same criteria for detecting ripples and fast ripples have been implemented by several groups (Staba et al., 2002; Gardner et al., 2007; Crepon et al., 2010; Zelmann et al., 2012). The mean rate of ripples (14.6 per minute) and fast

ripples (4.1 per minute) in this study was similar to previous studies where they visually identified HFAs in non-SOZ sites (ripples: 10.8 per minute; fast ripples: 2.0 per minute), further validating our automatic detector (Valenca et al., 2012).

The HFA characteristics were similar across all face-processing and land-processing regions, indicating that the detector was consistently detecting the same type of high frequency activity. However, another significance of this result was the opportunity to compare the HFAs in this study to previous studies, further validating our results as well as the detector. The distribution of peak spectral frequencies of the HFAs detected in this study were similar to that of the prior study implementing the RMS detector. The mean peak spectral frequency of ripples detected in this study was 95 Hz compared to a distribution centered at 96 Hz (Staba et al., 2002). The mean spectral frequency for fast ripples were slightly different, 275 Hz in this study compared to 260 Hz in a previous study (Staba et al., 2002). It must be noted that the HFAs detected in the Staba 2002 study were from microelectrodes in epileptogenic regions. However, it has been shown that macro-electrodes, such as the one used in this study, have a tendency to record events with peak frequencies that are slightly higher than those for micro-electrodes (Blanco et al., 2011).

The HFA durations in this study was different from the one by Staba and colleagues, but they matched that of a study describing spontaneous and visually driven HFAs (Nagasawa et al., 2012). The median duration of HFAs detected in this study (504 ms, 38 ms SD for ripples; 478 ms, 27 ms SD for fast ripples) were much longer than the duration of HFAs found by Staba and colleagues in 2002 (32.4 ms for ripples; 19.1 ms for fast ripples). This could be due to optimizing the detector to visually marked HFAs.

However, Nagasawa et al. found HFAs to have durations up to 1033 seconds (for ripples) and 577 ms (for fast ripples) during a visual task (2012). This indicates that it is possible that HFAs could have such long durations.

Furthermore, there was no significant difference in the rate of HFAs between the first and second half of fearful face blocks. This indicated that HFA was spread across the 24 second block and not just at the transition points, justifying using each block as a continuous stimulus to which the detected HFAs were binned. In face-induced ERPs, the amplitude returns to baseline within 1 second from presentation of face stimuli (Engel and Mccarthy 2011). Moreover, a face-specific late potential termed “AP350” potential originating from right ventral ATL following an earlier face-specific N200 originating from posterior ventral temporal cortex is reduced by the repetition of identical faces (Allison et. al. 1999; Puce et. al. 1999; Collins and Olson 2014). The consistency of HFA induction during face viewing may help differentiate whether the face processing nodes are part of the core or extended system.

The detected events presented in this study are more HFA than HFO. The difference between high frequency activity (HFA) and high frequency oscillation (HFO) is subtle but important. It has been proposed that studies refer to high frequency activity as “oscillations” only when there is evidence that the activity is rhythmic, or a collection of several rhythmic processes (Lachaux et al., 2012). Initially, we set out to detect HFOs, but after reviewing the detected events, we found that they were actually a combination of one or more rhythmic activity across several frequencies in the ripple and fast ripple band. This could also explain the long durations of the detected HFAs. This could mean that we have to perform further analysis on the detected events to

separate the “oscillations”; however, some events also indicated a broadband increase in the ripple and fast ripple band as opposed to a transient high frequency activity. This could be due to several factors, but we suspect it is most likely due to the modifications we implemented on the detector to improve performance and the gold standard used. Nevertheless, the proposed definition implies that HFOs are a subset of HFAs, therefore justifying the choice of using an HFO detector to identify transient high frequency oscillations that statistically stand out from the background activity,

A limitation of this this study was inadequate spatial sampling and precision due to the nature of the dataset. Because the subjects were epilepsy patients, the electrodes were placed solely for seizure localization. Channels found to be within close proximity to the SOZ were not included in the search for significant differences between landscape and faces. Precise localization, especially for surface electrodes, also presented a challenge to match with pre-surgical imaging because their presence deforms the brain. Moreover, the possibility of disease-related processes interfering with the reported high frequency activity cannot be ruled out completely, even after discarding the SOZ sites. However, the robustness of the HFA response to the change in stimuli – rate changes observed on a block-to-clock-basis – supports a physiological origin, and additional recordings can provide a more comprehensive picture of the face processing induced transient high frequency activity.

5 Summary

Here we presented evidence that transient HFAs were evoked in localized regions of the human brain during land and face perception. We defined HFAs as transient oscillations that stand out from background activity, and we validated and trained an automatic detector based on visually marked HFAs on a subset of our overall data. Additional validation comes from the similarity of the duration and peak spectral frequency of HFAs detected in this study to visually driven HFAs.

6 Future Work

We analyzed 465 intracranial EEG recordings from twelve subjects undergoing clinical evaluation for surgical treatment of epilepsy. The target locations of every implanted electrode were based solely on clinical requirements. Improving co-registration techniques of preimplantation MRI and post implantation CT could help with more precise electrode localization.

Moreover, as with every study involving cognition and implanted electrodes, the presence of epilepsy might confound the results. Investigating face-induced HFAs in healthy subjects through scalp EEG removes the confound of epileptic brain. Indeed, it has been established that fast oscillations could be found in scalp EEG (von Ellenreider et al., 2012; Melani et al., 2013; Zelman et al., 2014).

Investigating the relationship of face-induced HFAs to previously shown gamma oscillations and face-specific ERPs may provide more information on the precise roles of the different regions involved in face processing. In addition, further analysis could be done to characterize HFA events beyond their amplitude, frequency, and duration.

7 References

Allison T, Ginter H, McCarthy G, Nobre a C, Puce a, Luby M, Spencer DD (1994). Face recognition in human extrastriate cortex. J Neurophysiol 71:821–825.

Allison T, Puce A, Spencer DD, McCarthy G (1999). Electrophysiological studies of human face perception. I: Potentials generated in occipitotemporal cortex by face and non-face stimuli. Cereb Cortex 9:415–430.

Baker SN, Curio G, Lemon RN (2003). EEG oscillations at 600 Hz are macroscopic markers for cortical spike bursts. J Physiol 550:529–534.

Blanco, J. a, Stead, M., Krieger, A., Stacey, W., Maus, D., Marsh, E.,Worrell, G. a. (2011). Data mining neocortical high-frequency oscillations in epilepsy and controls. Brain : A Journal of Neurology, 134(Pt 10), 2948–59.

Bragin A, Engel J, Wilson CL, Fried I, Mathern GW (1999). Hippocampal and entorhinal cortex high-frequency oscillations (100-500 Hz) in human epileptic brain and in kainic acid-treated rats with chronic seizures. Epilepsia 40:127–137.

Buzsáki G, Horváth Z, Urioste R, Hetke J, Wise K (1992). High-frequency network oscillation in the hippocampus. Science 256:1025–1027.

Cohen MX. Analyzing Neural Time Series Data: Theory and Practice. Cambridge, MA: MIT Press, 2014.

Collins JA, Olson IR (2014). Beyond the FFA: The role of the ventral anterior temporal lobes in face processing. Neuropsychologia 61:65–79.

Crépon B, Navarro V, Hasboun D, Clemenceau S, Martinerie J, Baulac M, Adam C, Le Van Quyen M (2010). Mapping interictal oscillations greater than 200 Hz recorded with intracranial macroelectrodes in human epilepsy. Brain 133:33–45.

Crone NE, Korzeniewska A, Franaszczuk PJ (2011). Cortical γ responses: searching high and low. Int J Psychophysiol 79:9–15.

Engel AD, McCarthy G (2011). The relationship of gamma oscillations and face-specific ERPs recorded subdurally from occipitotemporal cortex. Cereb Cortex 21:1213–1221.

Epstein, R., & Kanwisher, N. (1998). A cortical representation of the local visual environment. Nature, 392(6676), 598–601.

Gardner AB, Worrell GA, Marsh E, Dlugos D, Litt B. (2007). Human and automated detection of high-frequency oscillations in clinical intracranial EEG recordings. Clinical Neurophysiol 118:1134–43.

Gray CM, Singer W (1989). Stimulus-specific neuronal oscillations in orientation columns of cat visual cortex. Proc Natl Acad Sci U S A 86:1698–1702.

Haxby, J. V., Ungerleider, L. G., Clark, V. P., Schouten, J. L., Hoffman, E. a., & Martin, A. (1999). The effect of face inversion on activity in human neural systems for face and object perception. Neuron, 22(1), 189–199.

Haxby JV., Hoffman E a., Gobbini MI (2000). The distributed human neural system for face perception. Trends Cogn Sci 4:223–233.

Jacobs J, LeVan P, Chander R, Hall J, Dubeau F, Gotman J (2008). Interictal high-frequency oscillations (80-500 Hz) are an indicator of seizure onset areas independent of spikes in the human epileptic brain. Epilepsia 49:1893–1907.

Klopp, J., Halgren, E., Marinkovic, K., Nenov, V., (1999). Face-selective spectral changes in the human fusiform gyrus. Clinical Neurophysiology 110, 676-682.

Kucewicz MT, Cimbalnik J, Matsumoto JY, Brinkmann BH, Bower MR, Vasoli V, Sulc V, Meyer F, Marsh WR, Stead SM, Worrell G a (2014). High frequency oscillations are associated with cognitive processing in human recognition memory. Brain 137:2231–2244.

Lachaux JP, George N, Tallon-Baudry C, Martinerie J, Hugueville L, Minotti L, Kahane P, Renault B (2005). The many faces of the gamma band response to complex visual stimuli. Neuroimage 25:491–501.

Lachaux, J.P., Axmacher, N., Mormann, F., Halgren, E., & Crone, N. E. (2012). High-frequency neural activity and human cognition: Past, present and possible future of intracranial EEG research. Progress in Neurobiology, 98(3), 279–301.

Matsumoto A, Brinkmann BH, Matthew Stead S, Matsumoto J, Kucewicz MT, Marsh WR, Meyer F, Worrell G (2013). Pathological and physiological high-frequency oscillations in focal human epilepsy. J Neurophysiol 110:1958–1964.

Melani, F., Zelmann, R., Dubeau, F., & Gotman, J. (2013). Occurrence of scalp-fast oscillations among patients with different spiking rate and their role as epileptogenicity marker. Epilepsy Research, 106(3), 345–356.

Nagasawa T, Juhász C, Rothermel R, Hoechstetter K, Sood S, Asano E (2012). Spontaneous and visually driven high-frequency oscillations in the occipital cortex: Intracranial recording in epileptic patients. Hum Brain Mapp 33:569–583.

Puce A, Allison T, McCarthy G (1999). Electrophysiological studies of human face perception. III: Effects of top-down processing on face-specific potentials. Cereb Cortex 9:445–458.

Riley JD, Fling BW, Cramer SC, Lin JJ (2015). Altered organization of face-processing networks in temporal lobe epilepsy. Epilepsia:n/a – n/a Available at: http://doi.wiley.com/10.1111/epi.12976.

Schacher M, Haemmerle B, Woermann FG, Okujava M, Huber D, Grunwald T, Krämer G, Jokeit H (2006). Amygdala fMRI lateralizes temporal lobe epilepsy. Neurology 66:81–87.

Staba RJ, Stead M, Worrell G a (2014). Electrophysiological biomarkers of epilepsy. Neurotherapeutics 11:334–346.

Staba RJ, Wilson CL, Bragin A, Fried I, Engel J (2002). Quantitative analysis of high-frequency oscillations (80-500 Hz) recorded in human epileptic hippocampus and entorhinal cortex. J Neurophysiol 88:1743–1752.

Von Ellenrieder, N., Andrade-Valença, L. P., Dubeau, F., & Gotman, J. (2012). Automatic detection of fast oscillations (40-200 Hz) in scalp EEG recordings. Clinical Neurophysiology : Official Journal of the International Federation of Clinical Neurophysiology, 123(4), 670–80.

Weiner KS, Grill-spector K (2015). The evolution of face processing networks. Trends Cogn Sci 19:1–2.

Worrell GA., Jerbi K, Kobayashi K, Lina JM, Zelmann R, Le Van Quyen M (2012). Recording and analysis techniques for high-frequency oscillations. Prog Neurobiol 98:265–278.

Zelmann, R., Mari, F., Jacobs, J., Zijlmans, M., Dubeau, F., & Gotman, J. (2012). A comparison between detectors of high frequency oscillations. Clinical Neurophysiology : Official Journal of the International Federation of Clinical Neurophysiology, 123(1), 106–16.

Zelmann, R., Lina, J. M., Schulze-Bonhage, a., Gotman, J., & Jacobs, J. (2014). Scalp EEG is not a blur: It can see high frequency oscillations although their generators are small. Brain Topography, 27(5), 683–704.